



Review

Mechanisms of Arrhythmias in the Brugada Syndrome

Michiel Blok ^{1,2} and Bastiaan J. Boukens ^{1,2,*} 

¹ Department of Medical Biology, Amsterdam University Medical Center, University of Amsterdam, 1105 AZ Amsterdam, The Netherlands; michiel.blok@kpn

² Department of Experimental Cardiology, Amsterdam University Medical Center, University of Amsterdam, 1105 AZ Amsterdam, The Netherlands

* Correspondence: b.j.boukens@amsterdamumc.nl; Tel.: +31-(0)20-566-4659

Received: 21 August 2020; Accepted: 21 September 2020; Published: 25 September 2020



Abstract: Arrhythmias in Brugada syndrome patients originate in the right ventricular outflow tract (RVOT). Over the past few decades, the characterization of the unique anatomy and electrophysiology of the RVOT has revealed the arrhythmogenic nature of this region. However, the mechanisms that drive arrhythmias in Brugada syndrome patients remain debated as well as the exact site of their occurrence in the RVOT. Identifying the site of origin and mechanism of Brugada syndrome would greatly benefit the development of mechanism-driven treatment strategies.

Keywords: RVOT; arrhythmia; Brugada syndrome; fibrosis

1. Introduction

The right ventricular outflow tract (RVOT) is the preferential site of origin of arrhythmias in the setting of Brugada syndrome, idiopathic ventricular tachycardia, and to a lesser extent arrhythmogenic right ventricular cardiomyopathy (ARVC) [1–6]. Although extensive research has provided compelling evidence in support of this observation, several fundamental questions remain unanswered: what intrinsic aspects of the RVOT make it a preferential site of arrhythmogenesis, and what pathophysiological mechanisms contribute to their occurrence?

Brugada syndrome is an inherited arrhythmic disorder characterized by an increased risk of ventricular tachycardia/ fibrillation and sudden cardiac death (SCD) [7]. The disorder is named after brothers Pedro and Josep Brugada who in their study of 1992 identified a subgroup of patients with recurrent episodes of aborted SCD but did not present overt structural heart disease [8]. These patients presented the right bundle branch block, short ventricular extrasystole coupled to polymorphic ventricular tachycardia, and a type 1 electrocardiogram (ECG) pattern consisting of a normal QT-interval but ST-segment elevation in the right precordial ECG (corresponding to leads V1–V3) [9]. Because of the variable nature of Brugada syndrome ECG and the fact it can even disappear temporarily, its manifestations are commonly provoked and unmasked with the sodium channel blockers ajmaline and flecainide [10–12].

Brugada syndrome is associated with a myriad of pathogenic mutations [7]. Genes affected by these mutations mainly encode for subunits of cardiac sodium, calcium, and potassium channels, but also regulators of these channels [13–15]. Loss-of-function mutations in the gene *SCN5A*, encoding the cardiac sodium channel $Na_v1.5$, are found in about 11–28% of Brugada syndrome patients but most frequent (about 62%) in the younger patients diagnosed (<17 years old) [13,16]. Currently, >300 distinct mutations have been uncovered in *SCN5A* of which most are localized in the transmembrane-spanning regions [13,17]. Even if genetically inherited, Brugada syndrome is usually diagnosed during adulthood when the ECG and arrhythmic manifestations become apparent [16,18,19]. Despite the current

evidence of its extensive genetic origin, the pathophysiological mechanism that causes life-threatening arrhythmias and SCD in Brugada syndrome remains a matter of debate [7,20].

In this review, we will discuss the current understanding of the mechanism and source of arrhythmias in the respective settings of Brugada syndrome. Firstly, this review will describe the unique aspects of the RVOT with respect to its anatomical structure, developmental background, and molecular characteristics. Second, we will summarize the scientific progress and discuss important findings relevant to understanding the mechanism underlying arrhythmias in Brugada syndrome.

2. The Right Ventricular Outflow Tract

2.1. Anatomy of the RVOT

The RVOT, also referred to as the free-standing muscular infundibular sleeve, is a thin smooth-walled tubular structure positioned between the pulmonary trunk and the right ventricular cavity, orientated cranial to the tricuspid valve (Figure 1). The RVOT can be divided into the anterior, left, right (free), and posterior (septal) walls; the latter is directly anterior to the LVOT and adjacent to the sinus of Valsalva [21]. Before birth, the process of OFT rotation results in the complex anatomical relationship between the RVOT and the LVOT. The RVOT wraps around the LVOT and their distal parts are positioned laterally relative to each other [21,22].

The RVOT wall is a multi-layered structure featuring three-dimensional networks of myofibers in a matrix of fibrous tissue. Here, the differences in the spatial orientation of these myofibers determine the complexity of the contractile motion of the heart. Compared to the right ventricle (RV) and LVOT, the spatial orientation of the RVOT myofiber bundles is different [23,24]. While its subepicardial layer is composed of circumferentially orientated myofibers, its middle and subendocardial layers are composed of myofibers running in a longitudinal direction, i.e., orientated to the long axis of the RVOT (Figure 1). This physiological variation in myofiber direction could, in theory, render the RVOT more vulnerable to myofiber disarray, particularly in the context of structural abnormalities. [25,26].

Between the left ventricle (LV) and RV, large differences exist in structural makeup including the distribution of fibrous tissue and fat. In the healthy human heart, the RV typically contains a greater collagen content compared to the LV, irrespective of age or sex [27,28]. Although in a recent report healthy tissue sections from the human RVOT were mentioned to be evaluated, unfortunately, no quantification of collagen content nor fat content in these specific sections were reported [28].

Similarly, fat is present in a healthy heart and typically most abundant in the RV wall, particularly at the level of the anterolateral and apical regions [29,30]. Besides presence at the epicardial surface, fat infiltrates the underlying myocardium (i.e., fatty infiltration) and localizes around vessels and nerves or separate strands of myocardial fibers [29]. It was found by Burke and colleagues that in human hearts with ARVC, intramyocardial fatty infiltration increased most extensively in the RVOT as well as the lateral apex [31]. Altogether, the question arises of what characteristics of RVOT render it a more vulnerable substrate to such structural abnormalities.

Using histology and two-photon microscopy, the RV wall of the mouse heart was previously found to be occupied by a higher number of non-vascular clefts, also of a bigger size, compared with the mouse LV wall [32]. This difference in tissue architecture was not accompanied by a significant difference in fibrosis levels [32]. Although the number and size of intramural clefts may affect the normal pathway of conduction in the RV and thereby cause a delay in transmural activation or conduction block, several key questions remain unanswered. Does the RV of the human heart similarly contain a higher number of intramural clefts than the LV? If the number of intramural clefts would indeed be directly proportional to the extent of conduction slowing and thus cause an arrhythmogenic substrate, does the RVOT contain more of such clefts than other anatomical structures of the heart [33]?

Anatomy of RVOT

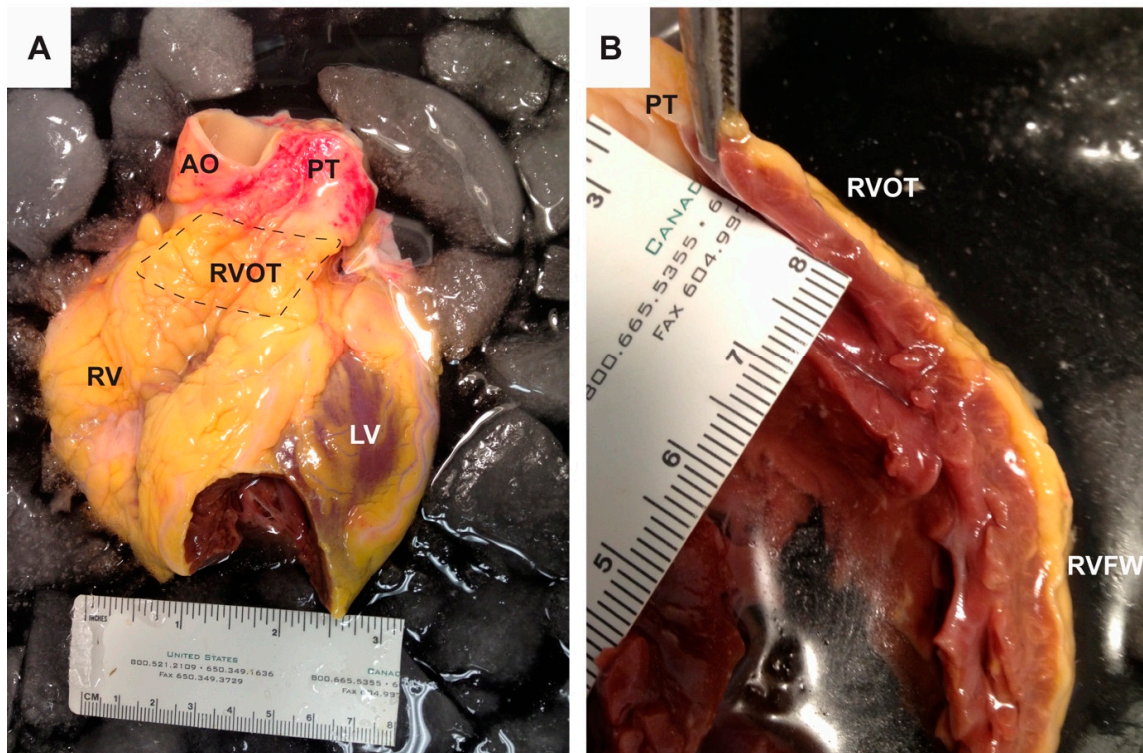


Figure 1. Anatomy of the right ventricular outflow tract (RVOT). The photographs are from a human heart of a male in his mid-fifties and taken by BJB. The heart was provided by Mid-America Transplant Services (St. Louis, MO, USA), as described previously [34], and its use was approved by the Washington University School of Medicine Ethics Committee [Institutional Review Board (IRB)]. Panel A shows the anterior side of the heart with RVOT indicated by the dashed box. Panel B is a photograph of a cross-section of the right ventricle showing the RVOT at the top. Note the absence of the trabecles at the lumen of the RVOT. RV, right ventricle; RVFW, right ventricular free wall; LV, left ventricle; AO, aorta; PT, pulmonary trunk.

2.2. Development of the RVOT

The RVOT, like the LVOT, stems from the embryonic structure referred to as the cardiac OFT. The morphogenesis of the cardiac OFT can be summarized into the following main steps: specification and proliferation of progenitors of the second heart field (SHF), differentiation of SHF progenitors into OFT tissue, migration of cardiac neural crest cells, OFT septation, and OFT rotation.

The cardiac OFT is derived from a subpopulation of cardiac progenitor cells that comprise the SHF and is the result of their continuous proliferation and addition to the primitive, linear heart tube (Figure 2) [35]. Consequently, rightward looping of the elongating heart tube contributes to it acquiring a more complex structure reminiscent to the definitive heart [36] and is followed by the formation of the early chambers as the myocardium of the heart tube bulges out (Figure 2) [37]. Meanwhile, as the newly formed chambers differentiate and acquire a secondary, or “working”, myocardial phenotype, the OFT myocardium retains its primary myocardial phenotype. While the properties of the working myocardium are associated with high expression of genes involved in respiratory-chain function, myofibril assembly, fast impulse conduction, and the contractile apparatus, primary myocardium marks nodal cells of the pacemaker and conduction system [38]. During fetal development, the RVOT differentiates into a more working myocardium phenotype, indicated by loss of expression of *Tbx2* [39]. Despite this, *Cx43* expression remains extinct in part of the RVOT after birth.

Migration and population of cardiac neural crest cells from the pharyngeal arches in the cardiac OFT contribute to its proper elongation, septation, rotation, and consequently proper arrangement of the LVOT and RVOT with respect to their respective ventricles [40–42].

Development of the RVOT

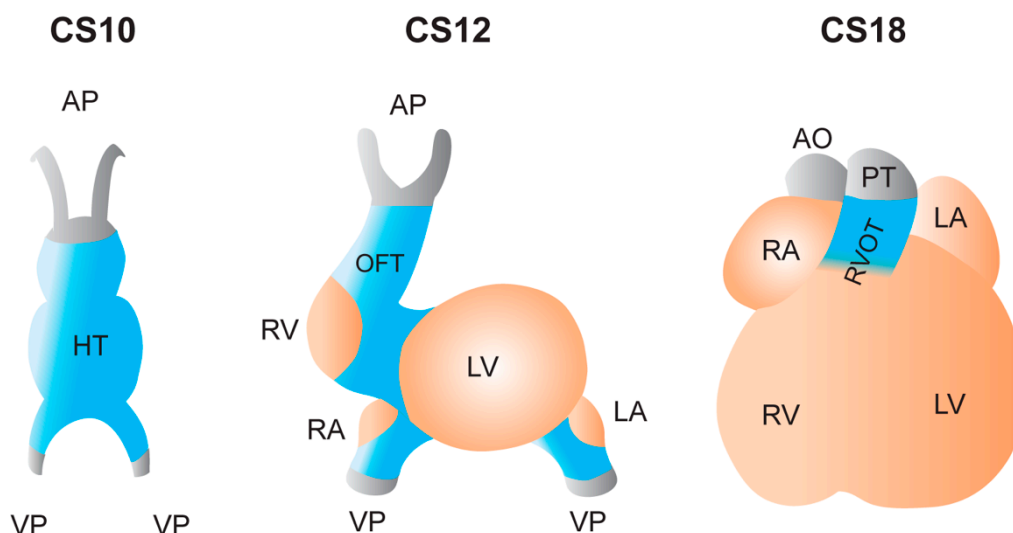


Figure 2. Development of the RVOT. Primary myocardium is indicated in blue and the embryonic working myocardium in orange. The embryonic outflow tract (OFT, composed of primary myocardium) gives rise to the (future) RVOT in the fetal and adult heart. During Carnegie stage (CS) 10, i.e., after 28 days of development, the arterial pole and venous poles of heart tube (HT) elongate by continuous proliferation and addition of cardiac progenitor cells. It is from CS10 that rightward looping of the linear heart tube initiates. During CS12 (i.e., day 30), as the heart tube loops, the cardiac chambers start to balloon out. At this stage, further elongation of the arterial pole has given rise to the tubular outflow tract (OFT) which connects the right ventricle (RV) to the aortic sac and aortic arches. During CS16 (i.e., day 39), the OFT has become relatively shorter with concomitant incorporation of its proximal part into the RV. Septation of the proximal OFT initiates at CS14, proceeds during CS16 by septation of the distal OFT, thereby giving rise to the pulmonary and aortic channels at CS18. At CS18 (i.e., day 44), the OFT is configured as for the postnatal heart. Both pulmonary and arterial components of the OFT are relative to each other in a spiral orientation. AP, arterial pole; VP, venous pole; LV, left ventricle; LA, left atrium; RA, right atrium; RVOT, right ventricular outflow tract; AO, aorta; PT, pulmonary trunk.

2.3. Molecular and Electrophysiological Makeup of the RVOT

Electrophysiological differences can be detected from apex-to-base as well as across the ventricular wall [34,37,39,43–49]. This electrophysiological pattern is the result of a complex network of inductive signals and transcription factors of which the expression is spatially and temporally regulated over the extent of early embryogenesis to postnatal maturation of the heart [50]. The gene regulatory network underlying the electrophysiological patterning of the RVOT remains largely unknown [51,52]. Just before birth, most of the RVOT myocardium acquires a working phenotype except for the subregion that is located just below the pulmonary valves (Figure 1) [37,39]. In the adult mouse heart, this myocardial subregion is marked by the absence of Cx43 expression, while the rest of the adult RVOT expresses Cx43 albeit at a lower level compared to the RV [53–55]. Despite its confined expression in the OFT and not the ventricular wall, and function as a transcriptional suppressor of the genes encoding the fast-conducting connexins Cx40 and Cx43 [50], Tbx2 was previously found not to regulate the expression of Cx43 in the RVOT [39]. Up to date, it is not completely understood what regulatory mechanism underlies the presence of this RVOT subregion [39]. Furthermore, *SCN5A* expression is

significantly lower in the adult mouse RVOT compared to the LV and RV. Although one may assume these electrophysiological characteristics would lead to conduction slowing, conduction velocity in the adult pig and mouse RVOT is similar to that in the RV [39,55,56].

While the electrophysiological heterogeneity throughout the RVOT itself may not necessarily explain why it is a preferential site of arrhythmogenesis, it may potentially render the RVOT a more susceptible region when electrophysiological changes would occur. For example, in *SCN5A*^{1798insd/+} adult mice, conduction was slowed to a larger extent in the RVOT compared to in the RV [39,57,58].

Genetic studies and subsequent functional follow-up studies have shed significant light on the key factors determining the electrophysiological characteristics of the RVOT [59]. In adult mice, heterozygous *Hey2* did not lead to abnormal ECGs nor structural heart disease. However, conduction velocity was significantly increased in the RVOT but not the RV nor LV free walls, underscoring an important role for HEY2 in determining the electrophysiological patterning of the RVOT [60]. HEY2 is a Notch-responsive transcription factor and an important regulator of cardiac muscle development, enriched in the subepicardium but not the subendocardium during embryogenesis while absent from the OFT [61–63]. The resultant transmural heterogeneity in HEY2 expression was shown to positively correlate with the transcriptional expression gradient of several ion channel- and gap junction-associated proteins including Na_v1.5 [60,63,64]. In the adult mouse heart, *Hey2* expression levels become indifferent from those in the LV and RV.

More recently, the GTPase RAS associated with Diabetes (RAD) was found to be expressed four-fold higher in the mouse RVOT compared with the LV and RV [65]. In addition, human RAD was found to be expressed in a transmural pattern, being higher in the subepicardium compared to endocardium in both ventricular compartments, suggesting that the same may apply to human RVOT myocardium [65]. In guinea pig ventricular cardiomyocytes, overexpression of a dominant-negative Rad mutant led to the upregulation of L-type calcium channel expression, resulting in a larger L-type calcium current density and prolongation of action potential duration [66]. These results may imply that RAD in the human RVOT regulates a lower L-type calcium channel expression in the subepicardium, thus resulting in a subepicardial action potential that is abbreviated compared to subendocardial action potentials.

3. Mechanisms Underlying Arrhythmias in Brugada Syndrome

3.1. The Settlement of the Debate about the Depolarization and Repolarization Hypothesis

Since the discovery of Brugada syndrome, controversy driven by a series of experimental findings supporting either of both the repolarization and conduction hypothesis caused considerable debate on what mechanism underlies Brugada syndrome pathophysiology [67–70]. In search of the cellular basis for Brugada syndrome, Yan and Antzelevitch and colleagues introduced in 1999 the concept of transmural dispersion of repolarization as the underlying cause of ST-segment elevation in the right precordial leads of the ECG [71]. Accordingly, this was due to a fundamental difference in transient outward current (I_{to}) which is intrinsically larger in the subepicardium in comparison to the subendocardium of the RV [72,73]. In combination with a reduction in depolarizing current, as such in the concomitant presence of an *SCN5A* loss-of-function mutation, this would result in loss of action potential dome and consequently phase-2 re-entry upon arrival of a subendocardial action potential wavefront (Figure 3) [13,17,74]. Later findings demonstrated that the electrophysiological manifestations of Brugada syndrome were most marked in the area around the RVOT [75–79].

Using activation mapping of the explanted human heart from a diagnosed Brugada syndrome patient Coronel and colleagues revealed the occurrence of significant conduction slowing in the RVOT, which was associated with a high degree of fatty infiltration and fibrosis in this region [80]. However, the characteristic inverted T wave was not present in all of the leads V1–V3 [81]. Furthermore, the presence of structural abnormality in the form of fibrofatty replacement did then not fit the Brugada syndrome description but rather favored the diagnosis of ARVC, albeit a genetic background associated

with ARVC could not be identified [81]. Using electroanatomic mapping, Nademanee and colleagues showed that within the anterior wall of the RVOT epicardium, radiofrequency ablation of abnormal regions displaying fractionated electrograms and conduction delay resulted in normalization of the Brugada syndrome ECG pattern in 8 out of 9 patients [82]. The late potentials observed in these electrograms were here assumed to arise as a result of delayed depolarization due to slow conduction, a notion that was supported by Sacher and colleagues several years later [83]. Szél and Antzelevitch challenged this (conduction) hypothesis by employing a pharmacological canine RV wedge model which was similar to the model used previously by Yan and Antzelevitch [71]. With this, they claimed to have successfully replicated the same electrogram fractionations as demonstrated in clinical cases [84]. Furthermore, they claimed that the occurrence of late potentials was rather due to an abbreviation in action potential duration in the subepicardium (Figure 3).

In 2017, a study by Leong and colleagues including 11 out of 13 patients tested positive for a Brugada syndrome ECG pattern after ajmaline challenge revealed that J-ST elevation positively correlated with an increasing conduction delay in the RVOT epicardium, but not in the RV [85]. Furthermore, heart rate-corrected activation recovery interval (ARI—index of myocardial action potential duration [86]) derived from the unipolar electrogram, was most prolonged in the RVOT compared to RV and LV following ajmaline challenge. However, in contrast to the earlier claimed, ARI prolongation in these cases did not correlate with the degree of J-ST elevation thus contradicting the repolarization hypothesis [87]. In response to this, Antzelevitch and Patocsikai expressed their alternative interpretation of these findings in support of the repolarization hypothesis, claiming that the negligible relative delay in conduction was not sufficient to account for the conduction hypothesis [85,88]. Rather, according to abnormal conduction, relative conduction should be roughly equivalent to the duration of ST-segment elevation.

Following their editorial, Patocsikai and colleagues used an experimental model, similar to that employed by Szél and Antzelevitch (see [84]), to show that the effect of ajmaline on conduction slowing was dependent on the magnitude of the action potential notch. The action potential notch was claimed to be the result of I_{to} activation [73,89]. Furthermore, epicardial radiofrequency ablation of RVOT regions that displayed abnormal electrograms successfully normalized the Brugada syndrome ECG pattern and abolished arrhythmic activity [89]. Furthermore, Patocsikai and colleagues showed that distinct late potentials developed as a result of concealed phase 2-reentry and a delay of the second action potential upstroke which were strictly dependent on the magnitude of the action potential notch [89].

Thus far, no report fully excluded the possibility of two seemingly opposing mechanisms occurring in the same setting. A critical point of debate however remains the fact that the repolarization hypothesis derives its support, not from the true setting occurring in patients, but mainly experimental models including canine ventricular wedge preparations which were previously found to fail in reproducing the same extent of arrhythmogenesis as in intact canine hearts [69,90,91]. One of the few clinical studies in support of the repolarization hypothesis, Morita and colleagues showed that in Brugada syndrome patients, leads corresponding to the RVOT consistently showed a longer QT interval of which dispersion was increased by blocking sodium current (I_{Na}) with pilsicainide [87,92]. Unfortunately, QT interval dispersion was not demonstrated in healthy subjects with the reason that such a control group could not be included [92].

To date, the current view based on accumulating evidence from clinical studies using electric mapping and body surface mapping strategies indicates that in Brugada syndrome patients with a type 1 ECG, (I) conduction in the RV/RVOT is slowed concomitant with significant activation delay, (II) there is an increase in the number of late potentials in the area of the RV/RVOT, and (III) changes in repolarization duration are not different compared to in healthy controls [93–98]. However, we think that in Brugada syndrome, genetic predisposition in the form of ion channel mutations involved in ventricular conduction does not solely determine arrhythmic risk but would rather modulate arrhythmic risk in the presence of 1 or more additional factors.

Mechanism of ST-segment elevation

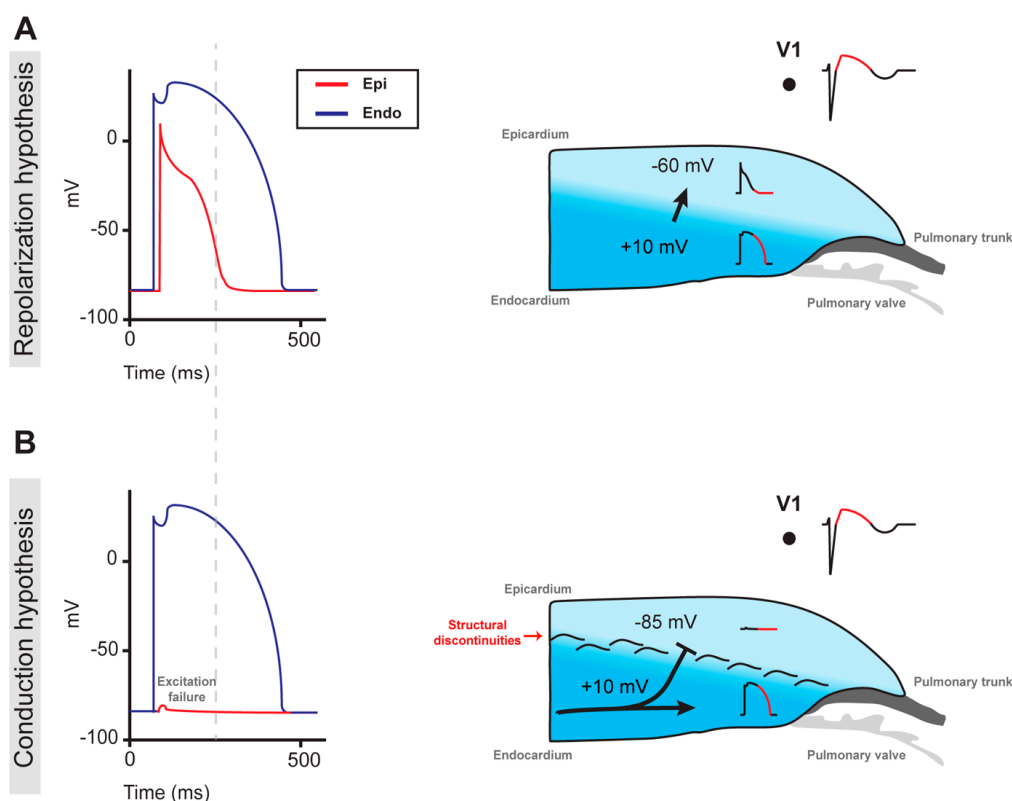


Figure 3. Mechanism of the ST-segment elevation in Brugada syndrome as postulated by the repolarization and conduction hypotheses. Action potentials from the subendocardial and subepicardial myocytes are indicated in blue and red respectively. (A) Transmural dispersion of repolarization, characterized by a loss of action potential dome in RVOT subepicardial myocytes, is caused by a reduced sodium current (I_{Na}) in combination with strong intrinsic expression of the transient outward current (I_{to}). (B) An abnormal pathway of conduction, imposed by subtle structural abnormalities throughout the RVOT myocardium, causes a current-to-load mismatch and conduction block which, in turn, leads to excitation failure of subepicardial myocytes.

3.2. Structural Abnormalities Appear Crucial for Explaining Arrhythmias in Brugada Syndrome

In 1989, Martini and colleagues presented on six patients with ventricular fibrillation without apparent structural heart disease but J point elevation in the ECG [99]. Interestingly, these patients described by Martini fit the diagnostic criteria for Brugada syndrome and showed structural abnormalities in the myocardium after careful reevaluation, leading Martini and colleagues to suggest that RV structural abnormalities underlie Brugada syndrome [100]. Since the discovery by Martini and colleagues, multiple lines of evidence have emerged in support of the presence of structural abnormalities in the hearts of Brugada syndrome patients which altogether led to the emergence of a new hypothesis for the Brugada syndrome pathophysiological mechanism, unifying the presence of structural abnormalities with reduced cardiac excitability [80,101–108].

Considering the increased presence of structural abnormalities in the RVOT wall of the Brugada syndrome heart [80,101–108], Hoogendijk and colleagues showed in 2010 how abnormal conduction in the structurally abnormal RV/RVOT could cause Brugada syndrome (Figure 3) [102]. According to their hypothesis, ST-segment elevation is the result of a current-to-load mismatch leading to excitation failure of the RV/RVOT subepicardium located distally to sites of an isthmus or sudden myocardial expansion and conduction block, formed by structural barriers in the form of fibrosis and fatty infiltration (Figure 3). A decrease in depolarizing current available for propagation (i.e., conduction

reserve [109] or safety factor for cardiac conduction [110]) would potentiate a higher number of sites of conduction block as indicated by further elevation of the ST-segment upon increasing ajmaline dose [103]. Alternatively, a decrease in long-type calcium current (I_{CaL}) or an increase in I_{to} would lead to a similar outcome [110–114]. The same area with structurally abnormal myocardium would disrupt the normal pathway of conduction, thus setting the stage for discontinuous impulse propagation causing activation delay because of the increased pathlength and electrogram fractionation (Figure 3). Via this abnormal conduction pathway, the propagating activation front would circle these sites of conduction block and cause re-entry, provided that activation distal to the site of conduction block is sufficiently delayed [115]. In turn, this re-entrant circuit would facilitate the development of self-perpetuating rapid and abnormal activation causing ventricular tachycardia, deteriorating into ventricular fibrillation, and asystole shortly after [116]. As described earlier, catheter ablation of such abnormal areas displaying fractionated electrograms in the anterior RVOT subepicardium should be highly efficient in eliminating the Brugada syndrome ECG pattern, provided that the intervention is executed adequately [82,117,118].

In 2015, Ten Sande and colleagues elaborate on this hypothesis, providing support using patient-derived findings that fractionated electrograms and ST-segment elevation in the RVOT is likely to arise in the same structurally abnormal subepicardium of the RV/RVOT region [102,111,119]. Electrogram fractionation was present in both Brugada syndrome patients and healthy controls but was less severe and not related to ST-segment elevation in the control group, suggesting that both phenomena arise by different mechanisms. A major drawback of their study was the absence of any documented evidence supporting the presence of structural abnormalities within the RVOT myocardium of their patient group [119]. The main bottleneck, as Ten Sande and colleagues pointed out in their communication [119], is the absence of conventional imaging techniques and diagnostic modalities capable of detecting the subtle structural abnormalities expected to be present in the RVOT architecture of live Brugada syndrome patients [102].

That structural abnormalities in the RVOT myocardium indeed can lead to excitation failure was demonstrated by Vigmond and colleagues by using a wedge preparation of the right ventricular wall from the heart of a 72-year-old female case without a history of cardiovascular disease [120]. The wedge preparation showed severe structural abnormalities characterized by fatty infiltration throughout the transmural wall, thereby dividing the RVOT myocardium into separate bundles. As a result, after activation of the proximal RVOT, local epicardial electrograms at the distal RVOT epicardium displayed fractionation and ST-segment elevation. Consistent with this, simulation of structural discontinuity at the margin of the distal RVOT area led to excitation failure of the same area. Despite the presence of fatty infiltration, the absence of fibrosis suggested that the donor likely did not suffer from ARVC and this was likely just a case of an aged heart [120].

4. Towards a Molecular Understanding of Brugada Syndrome

4.1. Known Genes Involved in the Brugada Syndrome Mechanism

Numerous mutations in, or genetics variants near, genes encoding proteins carrying ionic current have been discovered in Brugada syndrome patients [13–15]. Each of these genes can be seen as individual puzzle pieces which if put together reveal the puzzle that is the complex pathophysiological mechanism underlying Brugada syndrome. However, some genetic mutations or variants may occur commonly or rarely and are likely to vary in effect size. Only for a few of these genetic mutations and variants, the mechanism has been delineated.

Recently, whole-exome sequencing analysis identified *RRAD* as a novel gene associated with Brugada syndrome susceptibility [65]. Compared to control cells from an unaffected brother, induced pluripotent stem cell (iPSC)-derived cardiomyocytes derived from the index patient showed a severe decrease in I_{Na} , while I_{CaL} was moderately decreased (Figure 4) [65]. Furthermore, about 70% of these

cells presented with cytoskeletal defects reflected by an abnormal round shape and a reduced count of focal adhesion points (Figure 4) [65].

Through a genome-wide association study of 312 patients, Bezzina and colleagues previously identified three common genetic variants at the *SCN5A-SCN10A* and *HEY2* loci [63]. The identified variant in the *HEY2* locus was associated with an increased expression of HEY2 in the heart (Figure 4) [63]. Heterozygous loss of *Hey2* in mice resulted in increased conduction velocity in the RVOT compared to wildtype mice [63]. The following study by Veerman and colleagues showed that heterozygous loss of *Hey2* resulted in the loss of heterogeneity of I_{to} and I_{Na} densities between mouse RV subepicardial and subendocardial myocytes, although *SCN5A* expression was not significantly different compared to wildtype cells [60].

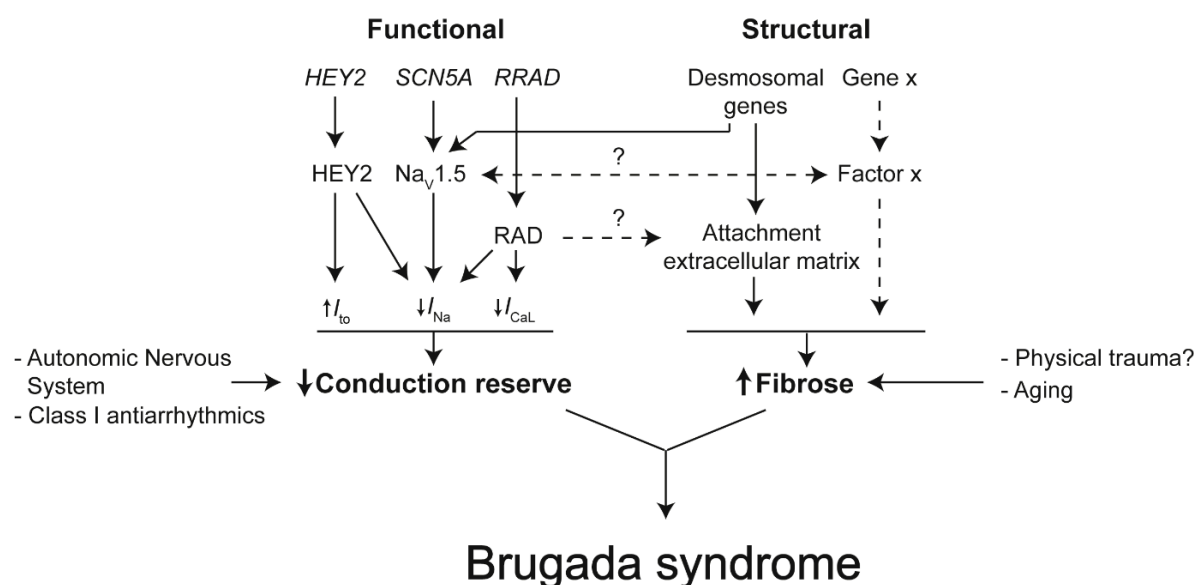


Figure 4. The working hypothesis underlying Brugada syndrome.

For the occurrence of Brugada syndrome, two components are required: (1) reduced conduction reserve and (2) structural abnormalities caused by interstitial fibrosis. Reduced conduction reserve can be due to a reduction in I_{Na} , and I_{CaL} or an increase in I_{to} [110]. Mutations in, or genetic variants near, genes encoding proteins carrying these currents have been found in Brugada syndrome patients [13–15]. Conduction reserve decreases by the administration of Class I antiarrhythmics (e.g., Ajmaline or Flecainide [12]) or by reduction of sympathetic activity [121]. In the presence of structural abnormalities, mainly caused by fibrosis, reduced conduction reserve can cause conduction delay or block [103]. The origin of interstitial fibrosis in Brugada syndrome patients is unclear. The sodium channel $Na_v1.5$ may, next to its electrogenic role, be involved in the formation of fibrosis [122,123]. It is also thought that RAD affects the attachment of cardiomyocytes to the extracellular matrix resulting in gaps between myocytes and space for fibrosis to form [65]. Genes encoding proteins important for securing desmosome integrity (e.g., PKP2) predispose to structural abnormalities and reduce I_{Na} in ARVC patients [124]. These proteins could play a relevant role in Brugada syndrome as well [125]. Interstitial fibrosis increases with which explains why Brugada syndrome is more prevalent in older people. Moreover, we think that the physical impact on the chest, or even the shape of the thorax, may cause interstitial fibrosis.

4.2. The Role of The Intercalated Disk in Reducing Conduction Reserve and Formation of Fibrosis

Despite classically defined as distinct clinical entities, Brugada syndrome and ARVC exhibit significant phenotypic overlap (for expert review, see reference [126]). In 1996, Corrado and colleagues reported an Italian family presenting ECG and clinical manifestations characteristic of Brugada

syndrome [8,99], while post-mortem analysis revealed adipose replacement of the RV free wall indicative of RV cardiomyopathy [108]. Brugada syndrome and ARVC both are associated with mutations encoding proteins of the intercalated disk. The cardiac intercalated disk hosts ion channel complexes including those consisting of $\text{Na}_V1.5$ channels [127]. While Brugada syndrome is associated most predominantly with loss-of-function mutations in the *SCN5A* gene (Figure 4), ARVC is a genetic myocardial disorder and most commonly associated with mutations in the *PKP2* gene encoding the desmosomal protein plakophilin-2 (PKP2), causing loss of integrity of the desmosome and disruption of structural coupling between adjacent cardiomyocytes [128–130]. As a result, *PKP2* mutations render cardiomyocytes more vulnerable to mechanical forces. The molecular mechanism underlying fibrotic formation and adipogenesis in ARVC likely involves PKP2 loss-of-function, given previous findings that loss of PKP2 knockdown leads to activation of signaling transduction pathways associated with transcriptional induction of genes that promote both forms of structural change [131,132].

Several *PKP2* mutations were previously identified in five unrelated individuals diagnosed with Brugada syndrome [133]. When transfected in HL-1 cells, these PKP2 mutants led to a decrease in I_{Na} density, likely caused by a defect of microtubule anchoring and $\text{Na}_V1.5$ trafficking to the intercalated disk (Figure 4) [133]. Such cytoskeletal abnormalities may precede or even give rise to larger-scale structural abnormalities on the tissue level. Besides PKP2, the presence of Cx43 at the intercalated disk was previously shown to be a prerequisite for microtubule-dependent trafficking of $\text{Na}_V1.5$ to the intercalated disk, as well as maintaining $\text{Na}_V1.5$ complexes [125,134–139]. On its part, the normal distribution of Cx43 at the intercalated disk relies on the presence of functional PKP2 [139,140]. Cx43 protein levels, quantified with immunofluorescence staining, were previously shown to be reduced at the intercalated disk in RVOT sections from Brugada syndrome patients compared to control hearts [104]. Furthermore, these RVOT sections showed increased epicardial surface fibrosis with some infiltrating the underlying myocardium causing interstitial myocardial fibrosis which was accompanied by focal replacement fibrosis [104]. In respect of whole hearts, the greatest collagen content was found in the RVOT epicardium [104]. Reducing Cx43 expression by about halve of total levels was previously shown to cause a reciprocal, significant increase in collagen deposition in the ventricles of aged mice but not the young [141]. Similarly, old but not young mice heterozygous for *SCN5A* showed an increased abundance of fibrosis in both cardiac ventricles with a reciprocal disturbance of the regular Cx43 distribution in and around areas containing fibrosis [142]. More recently, the *SCN5A*^{1798insD/+} mutation was demonstrated to cause structural abnormalities in the mouse embryo, thereby impairing ventricular activation before the onset of I_{Na} [122]. In Brugada syndrome patients, RV ejection fraction was recently found significantly lower compared to control subjects [98]. Furthermore, the same study showed that RV/RVOT areas with abnormal electrograms significantly correlated with the occurrence of mechanical dysfunction reflected by abnormal motion and deformation leading to wall stress [98]. Over time, such wall stress may facilitate the formation of structural abnormalities [98,102]. Collectively, these findings support an important contribution of cardiac aging to the formation of structural abnormalities in myocardial areas when the electromechanical coupling between cardiomyocytes is impaired, a notion that agrees with the conduction hypothesis postulating that structural abnormalities in Brugada syndrome are acquired throughout life explaining why the Brugada syndrome ECG is rare in children and more often manifests later in life [16,18,19,102].

Altogether, accumulating evidence has provided support to the notion that disruption of desmosome integrity (I) affects I_{Na} density, evidenced by a decreased amplitude of the I_{Na} in cardiomyocytes, (II) facilitates I_{Na} -dependent lethal arrhythmias in vivo, and (III) is likely to provide at least part of the molecular substrate of Brugada syndrome [125,133,134,143]. Furthermore, these findings should encourage the inclusion of *PKP2* as part of routine genetic testing for Brugada syndrome, in particular, to promote a better understanding of the key players participating in the molecular mechanism of this disorder. However, given the previous findings by Coronel and colleagues, the absence of an ARVC-associated genetic background whilst the presence of structural abnormalities

suggests that desmosomal defects associated with ARVC are not necessarily a prerequisite for the occurrence of structural abnormalities in Brugada syndrome [80,81].

4.3. Insights From Human Induced Pluripotent Stem Cell Models

The human iPSC technology has consistently been employed over the years to allow investigation of the molecular and cellular mechanism of Brugada syndrome in the setting of the native patient-specific cell environment. Despite this major advantage, human iPSC-derived cardiomyocyte models fail to capture the complex changes in tissue architecture that occur in Brugada syndrome. Nevertheless, human iPSC-derived cardiomyocytes are a useful tool to study the functional predisposition to Brugada syndrome. Collectively, these studies led to profound divergent results which could be explained by the variety of genetic mutations studied. In part, the effect of mutations may vary, even if affecting the same gene [144,145]. Furthermore, protocols for human iPSC-derived cardiomyocyte differentiation do not yield a pure cell population of a single type, but rather a variety of cardiomyocytes with divergent phenotypes. In addition, human iPSC-derived cardiomyocytes are characterized by their immature, fetal-like phenotype which, compared to adult cardiomyocytes, consists of different structural and functional properties [146].

While some studies reported no clear electrophysiological abnormalities in Brugada syndrome patient-derived iPSC-derived cardiomyocyte lines compared to controls [147,148], other reports contrarily showed evidence of significant alterations in action potential duration [65,144], decreased I_{Na} density [65,144,145,149–151], decreased action potential upstroke velocity [65,144,145,150,151], or irregular calcium handling [65,145]. Ma and colleagues found that pacing at a frequency of 0.1 Hz led to a small subgroup (25%) of Brugada syndrome patient-derived iPSC-derived cardiomyocytes presenting with action potentials which were by the authors claimed to resemble the loss of action potential dome configuration as postulated by the repolarization hypothesis, albeit the pacing frequency exceeding human physiological range [71,144]. Only a few studies focus on the potential presence of morphological changes, which were observed by Belbachir and colleagues in the form of cytoskeletal defects [65].

5. Summary

The scientific debate on the mechanism of Brugada syndrome has led to significant advancement in our understanding of its manifestations. The identification of structural abnormalities in the RVOT myocardium of Brugada syndrome patients has led to the current view that abnormal conduction as the pathophysiological mechanism. A multitude of factors would likely contribute to the presence of these structural abnormalities. Improvement of diagnostic imaging modalities and techniques could allow such subtle abnormalities to be detected in the hearts of Brugada syndrome patients both to help further progress the field and also to improve the management of Brugada syndrome patients. The current understanding of both ARVC and Brugada syndrome phenotypes hint toward a partial overlap in pathophysiological mechanisms causing structural abnormalities as seen in both disorders. Further investigation into this concept would improve the understanding of the underlying pathophysiology of the Brugada syndrome.

In conclusion, the RVOT is a unique structure in terms of anatomy and electrophysiology, which could explain why its preferential site of origin in the setting of Brugada syndrome. However, although various hypotheses have presented themselves over the last decades, the true answer remains concealed.

Author Contributions: M.B. and B.J.B. wrote the manuscript. Both authors have read and agreed to the published version of the manuscript. All authors have read and agreed to the published version of the manuscript.

Funding: This work was supported by the Dutch Heart Foundation (2016T047 to B.J.B.).

Conflicts of Interest: The authors declare no conflict of interest.

References

1. Haïssaguerre, M.; Extramiana, F.; Hocini, M.; Cauchemez, B.; Jaïs, P.; Cabrera, J.A.; Farre, G.; Leenhardt, A.; Sanders, P.; Scavée, C.; et al. Mapping and ablation of ventricular fibrillation associated with long-QT and brugada syndromes. *Circulation* **2003**, *108*, 925–928. [[CrossRef](#)] [[PubMed](#)]
2. Morita, H.; Nagase, S.; Miura, D.; Miura, A.; Hiramatsu, S.; Tada, T.; Murakami, M.; Nishii, N.; Nakamura, K.; Morita, S.T.; et al. Differential effects of cardiac sodium channel mutations on initiation of ventricular arrhythmias in patients with brugada syndrome. *Heart Rhythm* **2009**, *6*, 487–492. [[CrossRef](#)] [[PubMed](#)]
3. Marcus, F.I.; McKenna, W.J.; Sherrill, D.; Basso, C.; Bauce, B.; Bluemke, D.A.; Calkins, H.; Corrado, D.; Cox, M.G.P.J.; Daubert, J.P.; et al. Diagnosis of arrhythmogenic right ventricular cardiomyopathy/dysplasia: Proposed modification of the task force criteria. *Circulation* **2010**, *121*, 1533–1541. [[CrossRef](#)] [[PubMed](#)]
4. Viskin, S.; Rosso, R.; Rogowski, O.; Belhassen, B. The “short-coupled” variant of right ventricular outflow ventricular tachycardia: A not-so-benign form of benign ventricular tachycardia? *J. Cardiovasc. Electrophysiol.* **2005**, *16*, 912–916. [[CrossRef](#)] [[PubMed](#)]
5. Kim, R.J.; Iwai, S.; Markowitz, S.M.; Shah, B.K.; Stein, K.M.; Lerman, B.B. Clinical and electrophysiological spectrum of idiopathic ventricular outflow tract arrhythmias. *J. Am. Coll. Cardiol.* **2007**, *49*, 2035–2043. [[CrossRef](#)] [[PubMed](#)]
6. Buxton, A.E.; Waxman, H.L.; Marchlinski, F.E.; Simson, M.B.; Cassidy, D.; Josephson, M.E. Right ventricular tachycardia: Clinical and electrophysiologic characteristics. *Circulation* **1983**, *68*, 917–927. [[CrossRef](#)]
7. Sieira, J.; Dendramis, G.; Brugada, P. Pathogenesis and management of brugada syndrome. *Nat. Rev. Cardiol.* **2016**, *13*, 744–756. [[CrossRef](#)]
8. Brugada, P.; Brugada, J. Right bundle branch block, persistent ST segment elevation and sudden cardiac death: A distinct clinical and electrocardiographic syndrome. *Multicent. Rep. J. Am. Coll. Cardiol.* **1992**, *20*, 1391–1396. [[CrossRef](#)]
9. Wilde, A.A.M.; Antzelevitch, C.; Borggrefe, M.; Brugada, J.; Brugada, R.; Brugada, P.; Corrado, D.; Hauer, R.N.W.; Kass, R.S.; Nademanee, K.; et al. Proposed diagnostic criteria for the Brugada syndrome: Consensus report. *Circulation* **2002**, *106*, 2514–2519. [[CrossRef](#)]
10. Brugada, J.; Brugada, P. Further characterization of the syndrome of right bundle branch block, ST segment elevation, and sudden cardiac death. *J. Cardiovasc. Electrophysiol.* **1997**, *8*, 325–331. [[CrossRef](#)]
11. Rolf, S.; Bruns, H.J.; Wichter, T.; Kirchhof, P.; Ribbing, M.; Wasmer, K.; Paul, M.; Breithardt, G.; Haverkamp, W.; Eckardt, L. The ajmaline challenge in Brugada syndrome: Diagnostic impact, safety, and recommended protocol. *Eur. Heart J.* **2003**, *24*, 1104–1112. [[CrossRef](#)]
12. Antzelevitch, C.; Brugada, P.; Borggrefe, M.; Brugada, J.; Brugada, R.; Corrado, D.; Gussak, I.; LeMarec, H.; Nademanee, K.; Riera, A.R.P.; et al. Brugada syndrome: Report of the second consensus conference: Endorsed by the Heart Rhythm Society and the European Heart Rhythm Association. *Circulation* **2005**, *111*, 659–670. [[CrossRef](#)] [[PubMed](#)]
13. Kapplinger, J.D.; Tester, D.J.; Alders, M.; Benito, B.; Berthet, M.; Brugada, J.; Brugada, P.; Fressart, V.; Guerschicoff, A.; Harris-Kerr, C.; et al. An international compendium of mutations in the SCN5A-encoded cardiac sodium channel in patients referred for Brugada syndrome genetic testing. *Heart Rhythm* **2010**, *7*, 33–46. [[CrossRef](#)]
14. Nielsen, M.W.; Holst, A.G.; Olesen, S.P.; Olesen, M.S. The genetic component of brugada syndrome. *Front. Physiol.* **2013**, *4*, 179. [[CrossRef](#)]
15. Hu, D.; Barajas-Martínez, H.; Pfeiffer, R.; Dezi, F.; Pfeiffer, J.; Buch, T.; Betzenhauser, M.J.; Belardinelli, L.; Kahlig, K.M.; Rajamani, S.; et al. Mutations in SCN10A are responsible for a large fraction of cases of brugada syndrome. *J. Am. Coll. Cardiol.* **2014**, *64*, 66–79. [[CrossRef](#)]
16. Minier, M.; Probst, V.; Berthome, P.; Tixier, R.; Briand, J.; Geoffroy, O.; Clementy, N.; Mansourati, J.; Jesel, L.; Dupuis, J.M.; et al. Age at diagnosis of brugada syndrome: Influence on clinical characteristics and risk of arrhythmia. *Heart Rhythm* **2020**, *17*, 743–749. [[CrossRef](#)]
17. Sarquella-Brugada, G.; Campuzano, O.; Arbelo, E.; Brugada, J.; Brugada, R. Brugada syndrome: Clinical and genetic findings. *Genet. Med.* **2016**, *18*, 3–12. [[CrossRef](#)]
18. Andorin, A.; Behr, E.R.; Denjoy, I.; Crotti, L.; Dagradi, F.; Jesel, L.; Sacher, F.; Petit, B.; Mabo, P.; Maltret, A.; et al. Impact of clinical and genetic findings on the management of young patients with brugada syndrome. *Heart Rhythm* **2016**, *13*, 1274–1282. [[CrossRef](#)]

19. Oe, H.; Takagi, M.; Tanaka, A.; Namba, M.; Nishibori, Y.; Nishida, Y.; Kawarabayashi, T.; Yoshiyama, M.; Nishimoto, M.; Tanaka, K.; et al. Prevalence and clinical course of the juveniles with brugada-type ECG in Japanese population. *PACE-Pacing Clin. Electrophysiol.* **2005**, *28*, 549–554. [[CrossRef](#)]
20. Sieira, J.; Brugada, P. The definition of the Brugada syndrome. *Eur. Heart J.* **2017**, *38*, 3029–3034. [[CrossRef](#)]
21. Anderson, R.D.; Kumar, S.; Parameswaran, R.; Wong, G.; Voskoboinik, A.; Sugumar, H.; Watts, T.; Sparks, P.B.; Morton, J.B.; McLellan, A.; et al. Differentiating right-and left-sided outflow tract ventricular arrhythmias: Classical ECG signatures and prediction algorithms. *Circ. Arrhythmia Electrophysiol.* **2019**, *12*, e007392.
22. Asirvatham, S.J. Correlative anatomy for the invasive electrophysiologist: Outflow tract and supraventricular arrhythmia. *J. Cardiovasc. Electrophysiol.* **2009**, *20*, 955–968.
23. Ho, S.Y.; Nihoyannopoulos, P. Anatomy, echocardiography, and normal right ventricular dimensions. *Heart* **2006**, *92*, i2–i13.
24. Ghonim, S.; Voges, I.; Gatehouse, P.D.; Keegan, J.; Gatzoulis, M.A.; Kilner, P.J.; Babu-Narayan, S.V. Myocardial architecture, mechanics, and fibrosis in congenital heart disease. *Front. Cardiovasc. Med.* **2017**, *4*, 30. [[CrossRef](#)]
25. Roney, C.H.; Bayer, J.D.; Cochet, H.; Meo, M.; Dubois, R.; Jaïs, P.; Vigmond, E.J. Variability in pulmonary vein electrophysiology and fibrosis determines arrhythmia susceptibility and dynamics. *PLoS Comput. Biol.* **2018**, *14*, e1006166.
26. Roney, C.H.; Bayer, J.D.; Dubois, R.; Meo, M.; Cochet, H.; Jaïs, P.; Vigmond, E.J. The combination of pulmonary vein electrophysiology and atrial fibrosis determines driver location. In *Computing in Cardiology*; IEEE: Rennes, France, 2017.
27. Oken, D.E.; Boucek, R.J. Quantitation of collagen in human myocardium. *Circ. Res.* **1957**, *5*, 357–361.
28. Miles, C.; Westaby, J.; Ster, I.C.; Asimaki, A.; Boardman, P.; Joshi, A.; Papadakis, M.; Sharma, S.; Behr, E.R.; Sheppard, M.N. Morphometric characterization of collagen and fat in normal ventricular myocardium. *Cardiovasc. Pathol.* **2020**, *48*, 107224. [[CrossRef](#)]
29. Basso, C.; Thiene, G. Adipositas cordis, fatty infiltration of the right ventricle, and arrhythmogenic right ventricular cardiomyopathy. Just Matter Fat? *Cardiovasc. Pathol.* **2005**, *14*, 37–41. [[CrossRef](#)]
30. Tansey, D.K.; Aly, Z.; Sheppard, M.N. Fat in the right ventricle of the normal heart. *Histopathology* **2005**, *46*, 98–104.
31. Burke, A.P.; Farb, A.; Tashko, G.; Virmani, R. Arrhythmogenic right ventricular cardiomyopathy and fatty replacement of the right ventricular myocardium: Are they different diseases? *Circulation* **1998**, *97*, 1571–1580.
32. Kelly, A.; Salerno, S.; Connolly, A.; Bishop, M.; Charpentier, F.; Stølen, T.; Smith, G.L. Normal interventricular differences in tissue architecture underlie right ventricular susceptibility to conduction abnormalities in a mouse model of brugada syndrome. *Cardiovasc. Res.* **2018**, *114*, 724–736. [[CrossRef](#)] [[PubMed](#)]
33. Boukens, B.J.; Remme, C.A. Intramural clefts and structural discontinuities in brugada syndrome: The missing gap? *Cardiovasc. Res.* **2018**, *114*, 638–640. [[CrossRef](#)] [[PubMed](#)]
34. Boukens, B.J.; Sulkin, M.S.; Gloschat, C.R.; Ng, F.S.; Vigmond, E.J.; Efimov, I.R. Transmural APD gradient synchronizes repolarization in the human left ventricular wall. *Cardiovasc. Res.* **2015**, *108*, 188–196. [[CrossRef](#)] [[PubMed](#)]
35. Felker, A.; Prummel, K.D.; Merks, A.M.; Mickoleit, M.; Brombacher, E.C.; Huisken, J.; Panáková, D.; Mosimann, C. Continuous addition of progenitors forms the cardiac ventricle in zebrafish. *Nat. Commun.* **2018**, *9*, 2001. [[CrossRef](#)] [[PubMed](#)]
36. Desgrange, A.; Le Garrec, J.-F.; Meilhac, S.M. Left-right asymmetry in heart development and disease: Forming the right loop. *Development* **2018**, *145*, dev162776. [[CrossRef](#)]
37. Boukens, B.J.; Christoffels, V.M.; Coronel, R.; Moorman, A.F.M. Developmental basis for electrophysiological heterogeneity in the ventricular and outflow tract myocardium as a substrate for life-threatening ventricular arrhythmias. *Circ. Res.* **2009**, *104*, 19–31. [[CrossRef](#)]
38. van Eif, V.W.W.; Stefanovic, S.; van Duijvenboden, K.; Bakker, M.; Wakker, V.; de Gier-de Vries, C.; Zaffran, S.; Verkerk, A.O.; Boukens, B.J.; Christoffels, V.M. Transcriptome analysis of mouse and human sinoatrial node cells reveals a conserved genetic program. *Development* **2019**, *146*, dev173161. [[CrossRef](#)]
39. Boukens, B.J.; Sylva, M.; de Gier-de Vries, C.; Remme, C.A.; Bezzina, C.R.; Christoffels, V.M.; Coronel, R. Reduced sodium channel function unmasks residual embryonic slow conduction in the adult right ventricular outflow tract. *Circ. Res.* **2013**, *113*, 137–141. [[CrossRef](#)]

40. Yelbuz, T.M.; Waldo, K.L.; Kumiski, D.H.; Stadt, H.A.; Wolfe, R.R.; Leatherbury, L.; Kirby, M.L. Shortened outflow tract leads to altered cardiac looping after neural crest ablation. *Circulation* **2002**, *106*, 504–510. [[CrossRef](#)]
41. Bajolle, F.; Zaffran, S.; Kelly, R.G.; Hadchouel, J.; Bonnet, D.; Brown, N.A.; Buckingham, M.E. Rotation of the myocardial wall of the outflow tract is implicated in the normal positioning of the great arteries. *Circ. Res.* **2006**, *98*, 421–428. [[CrossRef](#)]
42. Inman, K.E.; Caiaffa, C.D.; Melton, K.R.; Sandell, L.L.; Achilleos, A.; Kume, T.; Trainor, P.A. Foxc2 is required for proper cardiac neural crest cell migration, outflow tract septation, and ventricle expansion. *Dev. Dyn.* **2018**, *247*, 1286–1296. [[CrossRef](#)] [[PubMed](#)]
43. Antzelevitch, C.; Sicouri, S.; Litovsky, S.H.; Lukas, A.; Krishnan, S.C.; Di Diego, J.M.; Gintant, G.A.; Liu, D.W. Heterogeneity within the ventricular wall. Electrophysiology and pharmacology of epicardial, endocardial, and M cells. *Circ. Res.* **1991**, *69*, 1427–1449. [[CrossRef](#)] [[PubMed](#)]
44. Viswanathan, P.C.; Shaw, R.M.; Rudy, Y. Effects of I(Kr) and I(Ks) heterogeneity on action potential duration and its rate dependence: A simulation study. *Circulation* **1999**, *99*, 2466–2474. [[CrossRef](#)] [[PubMed](#)]
45. Poelzing, S.; Akar, F.G.; Baron, E.; Rosenbaum, D.S. Heterogeneous connexin43 expression produces electrophysiological heterogeneities across ventricular wall. *Am. J. Physiol. Heart Circ. Physiol.* **2004**, *286*, H2001–H2009. [[CrossRef](#)]
46. Poelzing, S.; Rosenbaum, D.S. Altered connexin43 expression produces arrhythmia substrate in heart failure. *Am. J. Physiol. Heart Circ. Physiol.* **2004**, *287*, H1762–H1770. [[CrossRef](#)] [[PubMed](#)]
47. Strom, M.; Wan, X.; Poelzing, S.; Ficker, E.; Rosenbaum, D.S. Gap junction heterogeneity as mechanism for electrophysiologically distinct properties across the ventricular wall. *Am. J. Physiol. Heart Circ. Physiol.* **2010**, *298*, H787–H794. [[CrossRef](#)]
48. Gaborit, N.; Le Bouter, S.; Szuts, V.; Varro, A.; Escande, D.; Nattel, S.; Demolombe, S. Regional and tissue specific transcript signatures of ion channel genes in the non-diseased human heart. *J. Physiol.* **2007**, *582*, 675–693. [[CrossRef](#)]
49. Boukens, B.J.; Walton, R.; Meijborg, V.M.; Coronel, R. Transmural electrophysiological heterogeneity, the T-wave and ventricular arrhythmias. *Prog. Biophys. Mol. Biol.* **2016**, *122*, 202–214. [[CrossRef](#)]
50. Boukens, B.J.; Christoffels, V.M. Electrophysiological patterning of the heart. *Pediatr. Cardiol.* **2012**, *25*, 900–906. [[CrossRef](#)]
51. Harvey, R.P. Patterning the vertebrate heart. *Nat. Rev. Genet.* **2002**, *3*, 544–556. [[CrossRef](#)]
52. Black, B.L. Transcriptional pathways in second heart field development. *Semin. Cell Dev. Biol.* **2007**, *18*, 67–76. [[CrossRef](#)] [[PubMed](#)]
53. Boukens, B.J.; Coronel, R.; Christoffels, V.M. Embryonic development of the right ventricular outflow tract and arrhythmias. *Heart Rhythm* **2016**, *13*, 616–622. [[CrossRef](#)] [[PubMed](#)]
54. Aanhaanen, W.T.J.; Mommersteeg, M.T.M.; Norden, J.; Wakker, V.; de Gier-de Vries, C.; Anderson, R.H.; Kispert, A.; Moorman, A.F.M. Developmental origin, growth, and three-dimensional architecture of the atrioventricular conduction axis of the mouse heart. *Circ. Res.* **2010**, *107*, 728–736. [[CrossRef](#)] [[PubMed](#)]
55. Ou, B.; Nakagawa, M.; Kajimoto, M.; Nobe, S.; Ooie, T.; Ichinose, M.; Yonemochi, H.; Ono, N.; Shimada, T.; Saikawa, T. Heterogeneous expression of connexin 43 in the myocardium of rabbit right ventricular outflow tract. *Life Sci.* **2005**, *77*, 52–59. [[CrossRef](#)]
56. Park, D.S.; Cerrone, M.; Morley, G.; Vasquez, C.; Fowler, S.; Liu, N.; Bernstein, S.A.; Liu, F.Y.; Zhang, J.; Rogers, C.S.; et al. Genetically engineered SCN5A mutant pig hearts exhibit conduction defects and arrhythmias. *J. Clin. Investig.* **2015**, *125*, 403–412. [[CrossRef](#)]
57. Remme, C.A.; Verkerk, A.O.; Nuyens, D.; van Ginneken, A.C.G.; van Brunschot, S.; Belterman, C.N.W.; Wilders, R.; van Roon, M.A.; Tan, H.L.; Wilde, A.A.M.; et al. Overlap syndrome of cardiac sodium channel disease in mice carrying the equivalent mutation of human SCN5A-1795insD. *Circulation* **2006**, *114*, 2584–2594. [[CrossRef](#)]
58. Zhang, Y.; Guzhadur, L.; Jeevaratnam, K.; Salvage, S.C.; Matthews, G.D.K.; Lammers, W.J.; Lei, M.; Huang, C.L.H.; Fraser, J.A. Arrhythmic substrate, slowed propagation and increased dispersion in conduction direction in the right ventricular outflow tract of murine Scn5a+/- hearts. *Acta Physiol.* **2014**, *211*, 559–573. [[CrossRef](#)]
59. Heidecker, B. When high throughput meets mechanistic studies: A state-of-the-art approach in Brugada syndrome. *Circ. Res.* **2017**, *121*, 483–485. [[CrossRef](#)]

60. Veerman, C.C.; Podliesna, S.; Tadros, R.; Lodder, E.M.; Mengarelli, I.; de Jonge, B.; Beekman, L.; Barc, J.; Wilders, R.; Wilde, A.A.M.; et al. The brugada syndrome susceptibility gene HEY2 modulates cardiac transmural ion channel patterning and electrical heterogeneity. *Circ. Res.* **2017**, *121*, 537–548. [[CrossRef](#)]
61. Anderson, D.J.; Kaplan, D.I.; Bell, K.M.; Koutsis, K.; Haynes, J.M.; Mills, R.J.; Phelan, D.G.; Qian, E.L.; Leitoguinho, A.R.; Arasaratnam, D.; et al. NKX2-5 regulates human cardiomyogenesis via a HEY2 dependent transcriptional network. *Nat. Commun.* **2018**, *9*, 1373.
62. Miao, L.; Li, J.; Jun, L.; Tian, X.; Lu, Y.; Hu, S.; Shieh, D.; Kanai, R.; Zhou, B.-Y.; Zhou, B.; et al. Notch signaling regulates Hey2 expression in a spatiotemporal dependent manner during cardiac morphogenesis and trabecular specification. *Sci Rep.* **2018**, *8*, 2678. [[CrossRef](#)] [[PubMed](#)]
63. Bezzina, C.R.; Barc, J.; Mizusawa, Y.; Remme, C.A.; Gourraud, J.-B.; Simonet, F.; Verkerk, A.O.; Schwartz, P.J.; Crotti, L.; Dagradi, F.; et al. Common variants at SCN5A-SCN10A and HEY2 are associated with brugada syndrome, a rare disease with high risk of sudden cardiac death. *Nat. Genet.* **2013**, *45*, 1044–1049. [[CrossRef](#)] [[PubMed](#)]
64. Remme, C.A.; Verkerk, A.O.; Hoogaars, W.M.H.; Aanhaanen, W.T.J.; Scicluna, B.P.; Annink, C.; van den Hoff, M.J.B.; Wilde, A.A.M.; van Veen, T.A.B.; Veldkamp, M.W.; et al. The cardiac sodium channel displays differential distribution in the conduction system and transmural heterogeneity in the murine ventricular myocardium. *Basic Res. Cardiol.* **2009**, *104*, 511–522. [[CrossRef](#)] [[PubMed](#)]
65. Belbachir, N.; Portero, V.; Al Sayed, Z.R.; Gourraud, J.-B.; Dilasser, F.; Jesel, L.; Guo, H.; Wu, H.; Gaborit, N.; Guilluy, C.; et al. RRAD mutation causes electrical and cytoskeletal defects in cardiomyocytes derived from a familial case of brugada syndrome. *Eur. Heart J.* **2019**, *40*, 3081–3094. [[CrossRef](#)] [[PubMed](#)]
66. Yada, H.; Murata, M.; Shimoda, K.; Yuasa, S.; Kawaguchi, H.; Ieda, M.; Adachi, T.; Murata, M.; Ogawa, S.; Fukuda, K. Dominant negative suppression of Rad leads to QT prolongation and causes ventricular arrhythmias via modulation of L-type Ca²⁺ channels in the heart. *Circ. Res.* **2007**, *101*, 69–77. [[CrossRef](#)] [[PubMed](#)]
67. Brugada, R.; Roberts, R. Brugada Syndrome: Why are there multiple answers to a simple question? *Circulation* **2001**, *104*, 3017–3019. [[CrossRef](#)]
68. Meregalli, P.; Wilde, A.; Tan, H. Pathophysiological mechanisms of brugada syndrome: Depolarization disorder, repolarization disorder, or more? *Cardiovasc. Res.* **2005**, *67*, 367–378. [[CrossRef](#)]
69. Nademanee, K.; Wilde, A.A.M. Repolarization versus depolarization defects in brugada syndrome: A tale of 2 different electrophysiologic settings? *J. Am. Coll. Cardiol. Clin. Electrophysiol.* **2017**, *3*, 364–366.
70. Wilde, A.A.M.; Postema, P.G.; Di Diego, J.M.; Viskin, S.; Morita, H.; Fish, J.M.; Antzelevitch, C. The pathophysiological mechanism underlying brugada syndrome: Depolarization versus repolarization. *J. Mol. Cell. Cardiol.* **2010**, *49*, 543–553. [[CrossRef](#)]
71. Yan, G.X.; Antzelevitch, C. Cellular basis for the brugada syndrome and other mechanisms of arrhythmogenesis associated with ST-segment elevation. *Circulation* **1999**, *100*, 1660–1666. [[CrossRef](#)]
72. Lukas, A.; Antzelevitch, C. Differences in the electrophysiological response of canine ventricular epicardium and endocardium to ischemia: Role of the transient outward current. *Circulation* **1993**, *88*, 2903–2915. [[CrossRef](#)] [[PubMed](#)]
73. Di Diego, J.M.; Sun, Z.Q.; Antzelevitch, C. I(to) and action potential notch are smaller in left vs. Right canine ventricular epicardium. *Am. J. Physiol.* **1996**, *271*, H548–H561. [[CrossRef](#)] [[PubMed](#)]
74. Antzelevitch, C.; Belardinelli, L. The role of sodium channel current in modulating transmural dispersion of repolarization and arrhythmogenesis. *J. Cardiovasc. Electrophysiol. J. Cardiovasc. Electrophysiol.* **2006**, *17*, S79–S85. [[CrossRef](#)] [[PubMed](#)]
75. Eckardt, L.; Kirchhof, P.; Johna, R.; Breithardt, G.; Borggrefe, M.; Haverkamp, W. Transient local changes in right ventricular monophasic action potentials due to ajmaline in a patient with Brugada syndrome. *J. Cardiovasc. Electrophysiol.* **1999**, *10*, 1010–1015. [[CrossRef](#)]
76. Shimizu, W.; Matsuo, K.; Takagi, M.; Tanabe, Y.; Aiba, T.; Taguchi, A.; Suyama, K.; Kurita, T.; Aihara, N.; Kamakura, S. Body surface distribution and response to drugs of ST segment elevation in brugada syndrome: Clinical implication of eighty-seven-lead body surface potential mapping and its application to twelve-lead electrocardiograms. *J. Cardiovasc. Electrophysiol.* **2000**, *11*, 396–404. [[CrossRef](#)]

77. Takagi, M.; Aihara, N.; Kuribayashi, S.; Taguchi, A.; Shimizu, W.; Kurita, T.; Suyama, K.; Kamakura, S.; Hamada, S.; Takamiya, M. Localized right ventricular morphological abnormalities detected by electron-beam computed tomography represent arrhythmogenic substrates in patients with the brugada syndrome. *Eur. Heart J.* **2001**, *22*, 1032–1041. [[CrossRef](#)]
78. Kurita, T.; Shimizu, W.; Inagaki, M.; Suyama, K.; Taguchi, A.; Satomi, K.; Aihara, N.; Kamakura, S.; Kobayashi, J.; Kosakai, Y. The electrophysiologic mechanism of ST-segment elevation in brugada syndrome. *J. Am. Coll. Cardiol.* **2002**, *40*, 330–334. [[CrossRef](#)]
79. Veltmann, C.; Papavassiliou, T.; Konrad, T.; Doesch, C.; Kuschyk, J.; Streitner, F.; Haghi, D.; Michaely, H.J.; Schoenberg, S.O.; Borggrefe, M.; et al. Insights into the location of type I ECG in patients with brugada syndrome: Correlation of ECG and cardiovascular magnetic resonance imaging. *Heart Rhythm* **2012**, *9*, 414–421. [[CrossRef](#)]
80. Coronel, R.; Casini, S.; Koopmann, T.T.; Wilms-Schopman, F.J.G.; Verkerk, A.O.; de Groot, J.R.; Bhuiyan, Z.; Bezzina, C.R.; Veldkamp, M.W.; Linnenbank, A.C.; et al. Right ventricular fibrosis and conduction delay in a patient with clinical signs of brugada syndrome. *Circulation* **2005**, *112*, 2769–2777. [[CrossRef](#)]
81. Priori, S.G.; Napolitano, C.; Gasparini, M. Letters Regarding Article by Coronel et al. “Right ventricular fibrosis and conduction delay in a patient with clinical signs of brugada syndrome: A combined electrophysiological, genetic, histopathologic, and computational study”. *Circulation* **2005**, *113*, 2769–2777. [[CrossRef](#)]
82. Nademanee, K.; Veerakul, G.; Chandanamatha, P.; Chaothawee, L.; Ariyachaipanich, A.; Jirasirirojanakorn, K.; Likittanasombat, K.; Bhuripanyo, K.; Ngarmukos, T. Prevention of ventricular fibrillation episodes in brugada syndrome by catheter ablation over the anterior right ventricular outflow tract epicardium. *Circulation* **2011**, *123*, 1270–1279. [[PubMed](#)]
83. Sacher, F.; Jesel, L.; Jais, P.; Haïssaguerre, M. Insight into the mechanism of brugada syndrome: Epicardial substrate and modification during ajmaline testing. *Heart Rhythm* **2014**, *11*, 732–734. [[CrossRef](#)] [[PubMed](#)]
84. Szél, T.; Antzelevitch, C. Abnormal repolarization as the basis for late potentials and fractionated electrograms recorded from epicardium in experimental models of Brugada syndrome. *J. Am. Coll. Cardiol.* **2014**, *63*, 2037–2045. [[CrossRef](#)] [[PubMed](#)]
85. Leong, K.M.W.; Ng, F.S.; Yao, C.; Roney, C.; Taraborrelli, P.; Linton, N.W.F.; Whinnett, Z.I.; Lefroy, D.C.; Davies, D.W.; Boon Lim, P.; et al. ST-elevation magnitude correlates with right ventricular outflow tract conduction delay in type I brugada ECG. *Circ. Arrhythmia Electrophysiol.* **2017**, *10*, e005107.
86. Coronel, R.; de Bakker, J.M.T.; Wilms-Schopman, F.J.G.; Opthof, T.; Linnenbank, A.C.; Belterman, C.N.; Janse, M.J. Monophasic action potentials and activation recovery intervals as measures of ventricular action potential duration: Experimental evidence to resolve some controversies. *Heart Rhythm* **2006**, *3*, 1043–1050. [[CrossRef](#)]
87. Nagase, S.; Kusano, K.F.; Morita, H.; Nishii, N.; Banba, K.; Watanabe, A.; Hiramatsu, S.; Nakamura, K.; Sakuragi, S.; Ohe, T. Longer repolarization in the epicardium at the right ventricular outflow tract causes type 1 electrocardiogram in patients with brugada syndrome. *J. Am. Coll. Cardiol.* **2008**, *51*, 1154–1161.
88. Antzelevitch, C.; Patocskaï, B. Ajmaline-induced slowing of conduction in the right ventricular outflow tract cannot account for ST elevation in patients with type I brugada ECG. *Circ. Arrhythmia Electrophysiol.* **2017**, *10*, e005775.
89. Patocskaï, B.; Yoon, N.; Antzelevitch, C. Mechanisms underlying epicardial radiofrequency ablation to suppress arrhythmogenesis in experimental models of brugada syndrome. *JACC Clin. Electrophysiol.* **2017**, *3*, 353–363.
90. Janse, M.J.; Coronel, R.; Opthof, T.; Sosunov, E.A.; Anyukhovskiy, E.P.; Rosen, M.R. Repolarization gradients in the intact heart: Transmural or apico-basal? *Prog. Biophys. Mol. Biol.* **2012**, *109*, 6–15.
91. Boukens, B.J.; Meijborg, V.M.F.; Belterman, C.N.; Opthof, T.; Janse, M.J.; Schuessler, R.B.; Coronel, R.; Efimov, I.R. Local transmural action potential gradients are absent in the isolated, intact dog heart but present in the corresponding coronary-perfused wedge. *Physiol. Rep.* **2017**, *5*, e13251. [[CrossRef](#)]
92. Morita, H.; Zipes, D.P.; Fukushima-Kusano, K.; Nagase, S.; Nakamura, K.; Morita, S.T.; Ohe, T.; Wu, J. Repolarization heterogeneity in the right ventricular outflow tract: Correlation with ventricular arrhythmias in brugada patients and in an in vitro canine brugada model. *Heart Rhythm* **2008**, *5*, 725–733. [[CrossRef](#)] [[PubMed](#)]

93. Ohkubo, K.; Watanabe, I.; Takagi, Y.; Okumura, Y.; Ashino, S.; Kofune, M.; Kofune, T.; Shindo, A.; Sugimura, H.; Nakai, T.; et al. Endocardial electrograms from the right ventricular outflow tract after induced ventricular fibrillation in patients with brugada syndrome. *Circ. J.* **2007**, *71*, 1258–1262. [[CrossRef](#)] [[PubMed](#)]
94. Morita, H.; Kusano, K.F.; Miura, D.; Nagase, S.; Nakamura, K.; Morita, S.T.; Ohe, T.; Zipes, D.P.; Wu, J. Fragmented QRS as a marker of conduction abnormality and a predictor of prognosis of Brugada syndrome. *Circulation* **2008**, *118*, 1697–1704. [[CrossRef](#)]
95. Postema, P.G.; van Dessel, P.F.H.M.; de Bakker, J.M.T.; Dekker, L.R.C.; Linnenbank, A.C.; Hoogendijk, M.G.; Coronel, R.; Tijssen, J.G.P.; Wilde, A.A.M.; Tan, H.L. Slow and discontinuous conduction conspire in Brugada syndrome: A right ventricular mapping and stimulation study. *Circ. Arrhythmia Electrophysiol.* **2008**, *1*, 379–386. [[CrossRef](#)] [[PubMed](#)]
96. Postema, P.G.; van Dessel, P.F.H.M.; Kors, J.A.; Linnenbank, A.C.; van Herpen, G.; Ritsema van Eck, H.J.; van Geloven, N.; de Bakker, J.M.T.; Wilde, A.A.M.; Tan, H.L. Local depolarization abnormalities are the dominant pathophysiologic mechanism for type 1 electrocardiogram in brugada syndrome. A study of electrocardiograms, vectorcardiograms, and body surface potential maps during ajmaline provocation. *J. Am. Coll. Cardiol.* **2010**, *55*, 789–797. [[CrossRef](#)] [[PubMed](#)]
97. Letsas, K.P.; Efremidis, M.; Vlachos, K.; Georgopoulos, S.; Karamichalakis, N.; Asvestas, D.; Valkanas, K.; Korantzopoulos, P.; Liu, T.; Sideris, A. Right ventricular outflow tract high-density endocardial unipolar voltage mapping in patients with Brugada syndrome: Evidence for electroanatomical abnormalities. *Europace* **2018**, *20*, f57–f63. [[CrossRef](#)]
98. Pappone, C.; Mecarocci, V.; Manguso, F.; Ciconte, G.; Vicedomini, G.; Sturla, F.; Votta, E.; Mazza, B.; Pozzi, P.; Borrelli, V.; et al. New electromechanical substrate abnormalities in high-risk patients with Brugada syndrome. *Heart Rhythm* **2020**, *17*, 637–645. [[CrossRef](#)]
99. Martini, B.; Nava, A.; Thiene, G.; Buja, G.F.; Canciani, B.; Scognamiglio, R.; Daliento, L.; Dalla Volta, S. Ventricular fibrillation without apparent heart disease: Description of six cases. *Am. Heart J.* **1989**, *118*, 1203–1209. [[CrossRef](#)]
100. Martini, B.; Cannas, S.; Nava, A. Brugada by any other name? *Eur. Heart J.* **2001**, *22*, 1835–1836. [[CrossRef](#)]
101. Frustaci, A.; Priori, S.G.; Pieroni, M.; Chimenti, C.; Napolitano, C.; Rivolta, I.; Sanna, T.; Bellocchi, F.; Russo, M.A. Cardiac histological substrate in patients with clinical phenotype of brugada syndrome. *Circulation* **2005**, *112*, 3680–3687. [[CrossRef](#)]
102. Hoogendijk, M.G.; Opthof, T.; Postema, P.G.; Wilde, A.A.M.; de Bakker, J.M.T.; Coronel, R. The brugada ECG pattern: A marker of channelopathy, structural heart disease, or neither? Toward a unifying mechanism of the brugada syndrome. *Circ. Arrhythmia Electrophysiol.* **2010**, *3*, 283–290. [[CrossRef](#)] [[PubMed](#)]
103. Hoogendijk, M.G.; Potse, M.; Vinet, A.; de Bakker, J.M.T.; Coronel, R. ST segment elevation by current-to-load mismatch: An experimental and computational study. *Heart Rhythm* **2011**, *8*, 111–118. [[CrossRef](#)] [[PubMed](#)]
104. Nademanee, K.; Raju, H.; de Noronha, S.V.; Papadakis, M.; Robinson, L.; Rothery, S.; Makita, N.; Kowase, S.; Boonmee, N.; Vitayakritsirikul, V.; et al. Fibrosis, connexin-43, and conduction abnormalities in the brugada syndrome. *J. Am. Coll. Cardiol.* **2015**, *66*, 1976–1986. [[CrossRef](#)]
105. Zumhagen, S.; Spieker, T.; Rolinck, J.; Baba, H.A.; Breithardt, G.; Böcker, W.; Eckardt, L.; Paul, M.; Wichter, T.; Schulze-Bahr, E. Absence of pathognomonic or inflammatory patterns in cardiac biopsies from patients with brugada syndrome. *Circ. Arrhythmia Electrophysiol.* **2009**, *2*, 16–23. [[CrossRef](#)] [[PubMed](#)]
106. Ohkubo, K.; Watanabe, I.; Okumura, Y.; Takagi, Y.; Ashino, S.; Kofune, M.; Sugimura, H.; Nakai, T.; Kasamaki, Y.; Hirayama, A.; et al. Right ventricular histological substrate and conduction delay in patients with brugada syndrome. *Int. Heart J.* **2010**, *51*, 17–23. [[CrossRef](#)]
107. Tada, H.; Aihara, N.; Ohe, T.; Yutani, C.; Hamada, S.; Miyanuma, H.; Takamiya, M.; Kamakura, S. Arrhythmogenic right ventricular cardiomyopathy underlies syndrome of right bundle branch block, ST-segment elevation, and sudden death. *Am. J. Cardiol.* **1998**, *81*, 519–522. [[CrossRef](#)]
108. Corrado, D.; Nava, A.; Buja, G.; Martini, B.; Fasoli, G.; Oselladore, L.; Turrini, P.; Thiene, G. Familial cardiomyopathy underlies syndrome of right bundle branch block, ST segment elevation and sudden death. *J. Am. Coll. Cardiol.* **1996**, *27*, 443–448. [[CrossRef](#)]
109. van Rijen, H.V.M.; de Bakker, J.M.T. Penetrance of monogenetic cardiac conduction diseases. A matter of conduction reserve? *Cardiovasc. Res.* **2007**, *76*, 379–380. [[CrossRef](#)]

110. Boyle, P.M.; Franceschi, W.H.; Constantin, M.; Hawks, C.; Desplantez, T.; Trayanova, N.A.; Vigmond, E.J. New insights on the cardiac safety factor: Unraveling the relationship between conduction velocity and robustness of propagation. *J. Mol. Cell. Cardiol.* **2019**, *128*, 117–128. [[CrossRef](#)]
111. Hoogendijk, M.G.; Potse, M.; Linnenbank, A.C.; Verkerk, A.O.; den Ruijter, H.M.; van Amersfoorth, S.C.M.; Klaver, E.C.; Beekman, L.; Bezzina, C.R.; Postema, P.G.; et al. Mechanism of right precordial ST-segment elevation in structural heart disease: Excitation failure by current-to-load mismatch. *Heart Rhythm* **2010**, *7*, 238–248. [[CrossRef](#)]
112. Joyner, R.W.; Kumar, R.; Wilders, R.; Jongsma, H.J.; Verheijck, E.E.; Golod, D.A.; van Ginneken, A.C.G.; Wagner, M.B.; Goolsby, W.N. Modulating L-type calcium current affects discontinuous cardiac action potential conduction. *Biophys. J.* **1996**, *71*, 237–245. [[CrossRef](#)]
113. Rohr, S.; Kucera, J.P. Involvement of the calcium inward current in cardiac impulse propagation: Induction of unidirectional conduction block by nifedipine and reversal by bay K 8644. *Biophys. J.* **1997**, *72*, 754–766. [[CrossRef](#)]
114. Huelsing, D.J.; Spitzer, K.W.; Cordeiro, J.M.; Pollard, A.E. Conduction between isolated rabbit purkinje and ventricular myocytes coupled by a variable resistance. *Am. J. Physiol. Heart Circ. Physiol.* **1998**, *274*, H1163–H1173. [[CrossRef](#)] [[PubMed](#)]
115. Kléber, A.G.; Rudy, Y. Basic mechanisms of cardiac impulse propagation and associated arrhythmias. *Physiol. Rev.* **2004**, *84*, 431–488. [[CrossRef](#)]
116. Wellens, H.J.J.; Schwartz, P.J.; Lindemans, F.W.; Buxton, A.E.; Goldberger, J.J.; Hohnloser, S.H.; Huikuri, H.V.; Kääb, S.; La Rovere, M.T.; Malik, M. Risk stratification for sudden cardiac death: Current status and challenges for the future. *Eur. Heart J.* **2014**, *35*, 1642–1651. [[CrossRef](#)]
117. Zhang, P.; Tung, R.; Zhang, Z.; Sheng, X.; Liu, Q.; Jiang, R.; Sun, Y.; Chen, S.; Yu, L.; Ye, Y.; et al. Characterization of the epicardial substrate for catheter ablation of brugada syndrome. *Heart Rhythm* **2016**, *13*, 2151–2158. [[CrossRef](#)]
118. Veerakul, G.; Nademanee, K. Will we be able to cure brugada syndrome? *Heart Rhythm* **2016**, *13*, 2159–2160. [[CrossRef](#)]
119. Ten Sande, J.N.; Coronel, R.; Conrath, C.E.; Driessen, A.H.G.; de Groot, J.R.; Tan, H.L.; Nademanee, K.; Wilde, A.A.M.; de Bakker, J.M.T.; van Dessel, P.F.H.M. ST-segment elevation and fractionated electrograms in brugada syndrome patients arise from the same structurally abnormal subepicardial RVOT area but have a different mechanism. *Circ. Arrhythmia Electrophysiol.* **2015**, *8*, 1382–1392. [[CrossRef](#)]
120. Vigmond, E.J.; Efimov, I.R.; Rentschler, S.L.; Coronel, R.; Boukens, B.J. Fractionated electrograms with ST-segment elevation recorded from the human right ventricular outflow tract. *Heart Case Rep.* **2017**, *3*, 546–550. [[CrossRef](#)]
121. Kass, R.S.; Wiegers, S.E. The ionic basis of concentration-related effects of noradrenaline on the action potential of calf cardiac purkinje fibres. *J. Physiol.* **1982**, *322*, 541–558. [[CrossRef](#)]
122. Marchal, G.A.; Verkerk, A.O.; Mohan, R.A.; Wolswinkel, R.; Boukens, B.J.D.; Remme, C.A. The sodium channel NaV1.5 impacts on early murine embryonic cardiac development, structure and function in a non-electrogenic manner. *Acta Physiol.* **2020**. [[CrossRef](#)] [[PubMed](#)]
123. Rivaud, M.R.; Delmar, M.; Remme, C.A. Heritable arrhythmia syndromes associated with abnormal cardiac sodium channel function: Ionic and non-ionic mechanisms. *Cardiovasc. Res.* **2020**, *116*, 1557–1570. [[PubMed](#)]
124. Cerrone, M.; Delmar, M. Desmosomes and the sodium channel complex: Implications for arrhythmogenic cardiomyopathy and brugada syndrome. *Trends Cardiovasc. Med.* **2014**, *24*, 184–190. [[CrossRef](#)] [[PubMed](#)]
125. Cerrone, M.; Noorman, M.; Lin, X.; Chkourko, H.; Liang, F.X.; van der Nagel, R.; Hund, T.; Birchmeier, W.; Mohler, P.; van Veen, T.A.; et al. Sodium current deficit and arrhythmogenesis in a murine model of plakophilin-2 haploinsufficiency. *Cardiovasc. Res.* **2012**, *95*, 460–468. [[PubMed](#)]
126. Corrado, D.; Zorzi, A.; Cerrone, M.; Rigato, I.; Mongillo, M.; Bauce, B.; Delmar, M. Relationship between arrhythmogenic right ventricular cardiomyopathy and brugada syndrome. *Circ. Arrhythmia Electrophysiol.* **2016**, *9*, e003631.
127. Balse, E.; Steele, D.F.; Abriel, H.; Coulombe, A.; Fedida, D.; Hatem, S.N. Dynamic of ion channel expression at the plasma membrane of cardiomyocytes. *Physiol. Rev.* **2012**, *92*, 1317–1358.

128. Van Tintelen, J.P.; Entius, M.M.; Bhuiyan, Z.A.; Jongbloed, R.; Wiesfeld, A.C.P.; Wilde, A.A.M.; van der Smagt, J.; Boven, L.G.; Mannens, M.M.A.M.; van Langen, I.M.; et al. Plakophilin-2 mutations are the major determinant of familial arrhythmogenic right ventricular dysplasia/cardiomyopathy. *Circulation* **2006**, *113*, 1650–1658. [[CrossRef](#)]
129. Pieperhoff, S.; Schumacher, H.; Franke, W.W. The area composita of adhering junctions connecting heart muscle cells of vertebrates. V. The importance of plakophilin-2 demonstrated by small interference RNA-mediated knockdown in cultured rat cardiomyocytes. *Eur. J. Cell Biol.* **2008**, *87*, 399–411. [[CrossRef](#)]
130. Grossmann, K.S.; Grund, C.; Huelsken, J.; Behrend, M.; Erdmann, B.; Franke, W.W.; Birchmeier, W. Requirement of plakophilin 2 for heart morphogenesis and cardiac junction formation. *J. Cell Biol.* **2004**, *167*, 149–160.
131. Chen, S.N.; Gurha, P.; Lombardi, R.; Ruggiero, A.; Willerson, J.T.; Marian, A.J. The hippo pathway is activated and is a causal mechanism for adipogenesis in arrhythmogenic cardiomyopathy. *Circ. Res.* **2014**, *114*, 454–468. [[CrossRef](#)]
132. Dubash, A.D.; Kam, C.Y.; Aguado, B.A.; Patel, D.M.; Delmar, M.; Shea, L.D.; Green, K.J. Plakophilin-2 loss promotes TGF- β 1/p38 MAPK-dependent fibrotic gene expression in cardiomyocytes. *J. Cell Biol.* **2016**, *212*, 425–438. [[CrossRef](#)] [[PubMed](#)]
133. Cerrone, M.; Lin, X.; Zhang, M.; Agullo-Pascual, E.; Pfenniger, A.; Chkourko Gusky, H.; Novelli, V.; Kim, C.; Tirasawadichai, T.; Judge, D.P.; et al. Missense mutations in plakophilin-2 cause sodium current deficit and associate with a brugada syndrome phenotype. *Circulation* **2014**, *129*, 1092–1103. [[CrossRef](#)] [[PubMed](#)]
134. Sato, P.Y.; Coombs, W.; Lin, X.; Nekrasova, O.; Green, K.J.; Isom, L.L.; Taffet, S.M.; Delmar, M. Interactions between ankyrin-G, plakophilin-2, and connexin43 at the cardiac intercalated disc. *Circ. Res.* **2011**, *109*, 193–201. [[CrossRef](#)]
135. Jansen, J.A.; Noorman, M.; Musa, H.; Stein, M.; de Jong, S.; van der Nagel, R.; Hund, T.J.; Mohler, P.J.; Vos, M.A.; van Veen, T.A.; et al. Reduced heterogeneous expression of Cx43 results in decreased Nav1.5 expression and reduced sodium current that accounts for arrhythmia vulnerability in conditional Cx43 knockout mice. *Heart Rhythm* **2012**, *9*, 600–607. [[CrossRef](#)]
136. Lübke-meier, I.; Requardt, R.P.; Lin, X.; Sasse, P.; Andrié, R.; Schrickel, J.W.; Chkourko, H.; Bukauskas, F.F.; Kim, J.S.; Frank, M.; et al. Deletion of the last five C-terminal amino acid residues of connexin43 leads to lethal ventricular arrhythmias in mice without affecting coupling via gap junction channels. *Basic Res. Cardiol.* **2013**, *108*, 348. [[CrossRef](#)]
137. Agullo-Pascual, E.; Lin, X.; Leo-Macias, A.; Zhang, M.; Liang, F.X.; Li, Z.; Pfenniger, A.; Lübke-meier, I.; Keegan, S.; Fenyó, D.; et al. Super-resolution imaging reveals that loss of the C-terminus of connexin43 limits microtubule plus-end capture and Nav1.5 localization at the intercalated disc. *Cardiovasc. Res.* **2014**, *104*, 371–381. [[CrossRef](#)] [[PubMed](#)]
138. Desplantez, T.; McCain, M.L.; Beauchamp, P.; Rigoli, G.; Rothen-Rutishauser, B.; Parker, K.K.; Kléber, A.G. Connexin43 ablation in foetal atrial myocytes decreases electrical coupling, partner connexins, and sodium current. *Cardiovasc. Res.* **2012**, *94*, 58–65. [[CrossRef](#)]
139. Noorman, M.; Hakim, S.; Kessler, E.; Groeneweg, J.A.; Cox, M.G.P.J.; Asimaki, A.; van Rijen, H.V.M.; van Stuijvenberg, L.; Chkourko, H.; van der Heyden, M.A.G.; et al. Remodeling of the cardiac sodium channel, connexin43, and plakoglobin at the intercalated disk in patients with arrhythmogenic cardiomyopathy. *Heart Rhythm* **2013**, *10*, 412–419. [[CrossRef](#)]
140. Fidler, L.M.; Wilson, G.J.; Liu, F.; Cui, X.; Scherer, S.W.; Taylor, G.P.; Hamilton, R.M. Abnormal connexin43 in arrhythmogenic right ventricular cardiomyopathy caused by plakophilin-2 mutations. *J. Cell Mol. Med.* **2009**, *13*, 4219–4228. [[CrossRef](#)]
141. Jansen, J.A.; van Veen, T.A.B.; de Jong, S.; van der Nagel, R.; van Stuijvenberg, L.; Driessen, H.; Labzowski, R.; Oefner, C.M.; Bosch, A.A.; Nguyen, T.Q.; et al. Reduced Cx43 expression triggers increased fibrosis due to enhanced fibroblast activity. *Circ. Arrhythmia Electrophysiol.* **2012**, *5*, 380–390. [[CrossRef](#)]
142. Royer, A.; van Veen, T.A.B.; Le Bouter, S.; Marionneau, C.; Griol-Charhbil, V.; Léoni, A.L.; Steenman, M.; van Rijen, H.V.M.; Demolombe, S.; Goddard, C.A.; et al. Mouse model of SCN5A-linked hereditary Lenègre's: Disease age-related conduction slowing and myocardial fibrosis. *Circulation* **2005**, *111*, 1738–1746.
143. Sato, P.Y.; Musa, H.; Coombs, W.; Guerrero-Serna, G.; Patiño, G.A.; Taffet, S.M.; Isom, L.L.; Delmar, M. Loss of plakophilin-2 expression leads to decreased sodium current and slower conduction velocity in cultured cardiac myocytes. *Circ. Res.* **2009**, *105*, 523–526. [[CrossRef](#)] [[PubMed](#)]

144. Ma, D.; Liu, Z.; Loh, L.J.; Zhao, Y.; Li, G.; Liew, R.; Islam, O.; Wu, J.; Chung, Y.Y.; Teo, W.S.; et al. Identification of an I_{Na}-dependent and I_{to}-mediated proarrhythmic mechanism in cardiomyocytes derived from pluripotent stem cells of a Brugada syndrome patient. *Sci. Rep.* **2018**, *8*, 11246. [[CrossRef](#)] [[PubMed](#)]
145. Liang, P.; Sallam, K.; Wu, H.; Li, Y.; Itzhaki, I.; Garg, P.; Zhang, Y.; Vermglinchan, V.; Lan, F.; Gu, M.; et al. Patient-specific and genome-edited induced pluripotent stem cell-derived cardiomyocytes elucidate single-cell phenotype of brugada syndrome. *J. Am. Coll. Cardiol.* **2016**, *68*, 2086–2096. [[CrossRef](#)] [[PubMed](#)]
146. Ahmed, R.E.; Anzai, T.; Chanthra, N.; Uosaki, H. A brief review of current maturation methods for human induced pluripotent stem cells-derived cardiomyocytes. *Front. Cell Dev. Biol.* **2020**, *8*, 178. [[CrossRef](#)] [[PubMed](#)]
147. Veerman, C.C.; Mengarelli, I.; Guan, K.; Stauske, M.; Barc, J.; Tan, H.L.; Wilde, A.A.M.; Verkerk, A.O.; Bezzina, C.R. hiPSC-derived cardiomyocytes from Brugada Syndrome patients without identified mutations do not exhibit clear cellular electrophysiological abnormalities. *Sci. Rep.* **2016**, *6*, 30967. [[CrossRef](#)] [[PubMed](#)]
148. Miller, D.C.; Harmer, S.C.; Poliandri, A.; Nobles, M.; Edwards, E.C.; Ware, J.S.; Sharp, T.V.; McKay, T.R.; Dunkel, L.; Lambiase, P.D.; et al. Ajmaline blocks I_{Na} and I_{Kr} without eliciting differences between brugada syndrome patient and control human pluripotent stem cell-derived cardiac clusters. *Stem Cell Res.* **2017**, *25*, 233–244. [[CrossRef](#)] [[PubMed](#)]
149. Selga, E.; Sendfeld, F.; Martinez-Moreno, R.; Medine, C.N.; Tura-Ceide, O.; Wilmut, S.I.; Pérez, G.J.; Scornik, F.S.; Brugada, R.; Mills, N.L. Sodium channel current loss of function in induced pluripotent stem cell-derived cardiomyocytes from a Brugada syndrome patient. *J. Mol. Cell. Cardiol.* **2018**, *114*, 10–19. [[CrossRef](#)]
150. El-Battrawy, I.; Müller, J.; Zhao, Z.; Cyganek, L.; Zhong, R.; Zhang, F.; Kleinsorge, M.; Lan, H.; Li, X.; Xu, Q.; et al. Studying brugada syndrome with an scn1b variants in human-induced pluripotent stem cell-derived cardiomyocytes. *Front. Cell Dev. Biol.* **2019**, *7*, 261. [[CrossRef](#)] [[PubMed](#)]
151. El-Battrawy, I.; Albers, S.; Cyganek, L.; Zhao, Z.; Lan, H.; Li, X.; Xu, Q.; Kleinsorge, M.; Huang, M.; Liao, Z.; et al. A cellular model of Brugada syndrome with SCN10A variants using human-induced pluripotent stem cell-derived cardiomyocytes. *Europace* **2019**, *21*, 1410–1421. [[CrossRef](#)]



© 2020 by the authors. Licensee MDPI, Basel, Switzerland. This article is an open access article distributed under the terms and conditions of the Creative Commons Attribution (CC BY) license (<http://creativecommons.org/licenses/by/4.0/>).